Understanding the Impact of Raw Material Variation on Investment Casting Refractories

Emma Jones[a], Professor Stuart Blackburn[a], Dr Jeffery Knight[b], Dr Stewart Welch[b]

[a]School of Chemical Engineering, University of Birmingham, Edgbaston, B15 2TT
[b]Rolls-Royce Plc, Precision Casting Facility, Wilmore Road, Derby, DE24 9BD

1 Project Overview

As the demand for more efficient engines increases for Rolls-Royce (R-R), it is important to ensure continuity of supply of raw materials. In addition, as parts are becoming more complex, there are now tighter dimensional control requirements and any change in the raw material's chemical and physical properties can lead to significant changes in dimensional and process yields.

As these changes are inevitable, it is important to understand the relationship between the raw material properties, the behaviour through R-R's manufacturing process and the key final part attributes. From this understanding, the aim of this project is to create an appropriate strategic plan to manage the raw material supply chain risks at the lowest cost by applying formulation engineering principles.

2 Investment Casting Process

The turbine blades produced by R-R are manufactured by the investment casting process as its high precision offers near or net near shape components. The overall process is illustrated in the figure below [1]:

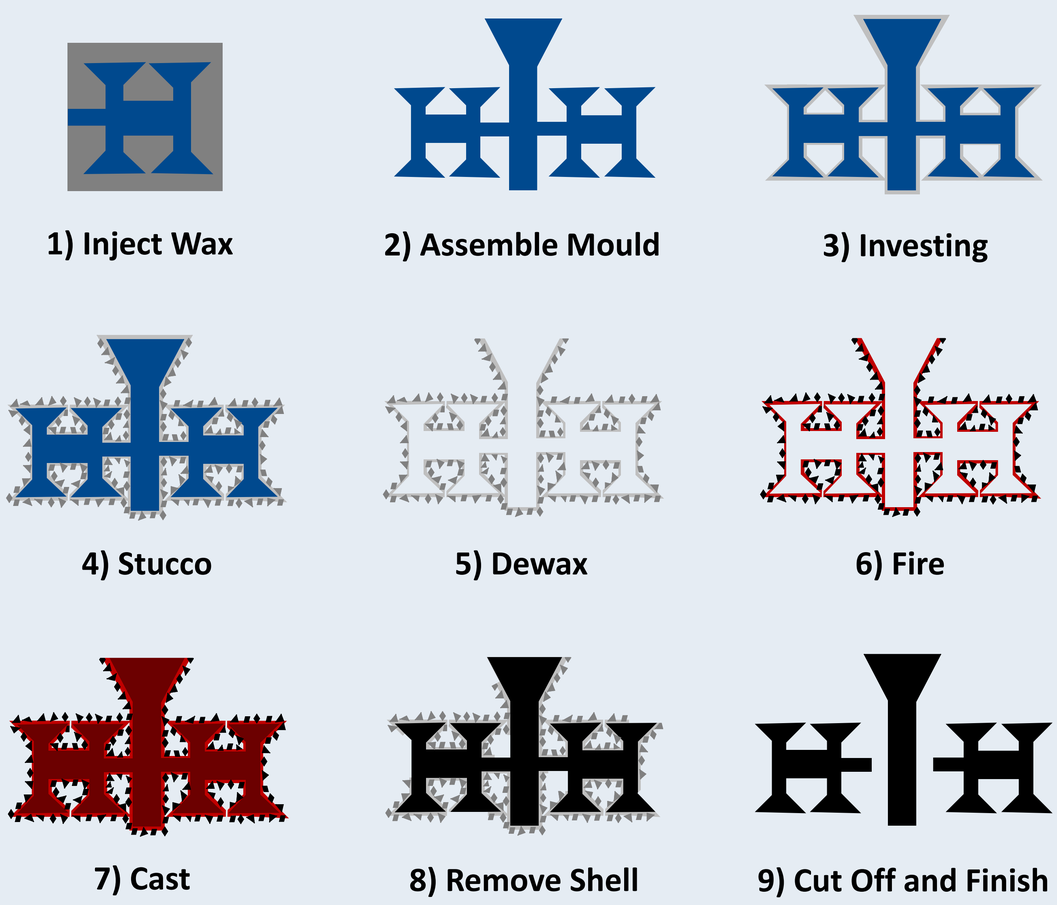

Figure 1: Systematic of basic investment casting process [1].

3 The Material

To formulate a suitable ceramic shell, zircon ($ZrSiO_4$) is used as the filler material as it possesses several desirable properties such as [2]:

- Low thermal expansion
- High thermal conductivity
- High melting point
- Chemical stability

Figure 2: Chosen mining locations for zircon grades to be investigated.

There are various grades of zircon available which can be purchased from different locations; each with particular chemistries and physical properties. The effect of mining location on raw material properties will be investigated by characterising zircon powders from all over the world, as shown in Figure 2.

4 Characterisation Techniques

This project will look at a variety of commercially available zircon powders in order to characterise the effect of mining location and processing on fundamental physical and chemical properties:

	1 Particle size distribution	2 Impurities present	3 Chemistry
Aim	Consider what effect a coarser PSD will have on dimensional control and variability between shells.	Identify which impurities are present, where they are located within the crystal structure and explore what effect they have on the shell system.	Investigate what influence calcination and radiation damage have on the crystal structure.
Action	Produce a bespoke PSD. Compare fine vs coarse – develop test bars.	Compare impurities in differently sourced zircons. Synthetically produce zircon and dope it with varying concentrations of impurities.	Measure the radioactivity of the differently sourced zircons. Obtain a non-calcined zircon, measure its radioactivity, calcine it and then irradiate it.

Figure 3: Main material properties to investigate.

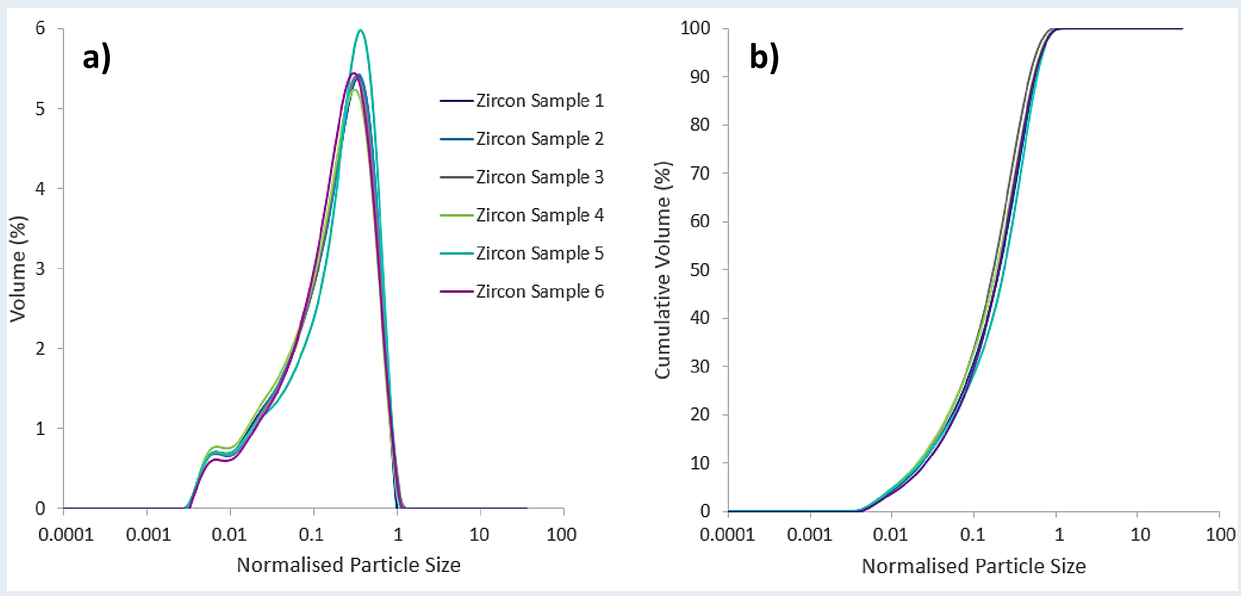

Figure 4: a) PSD volume and b) PSD cumulative volume distribution of six differently sourced zircon samples.

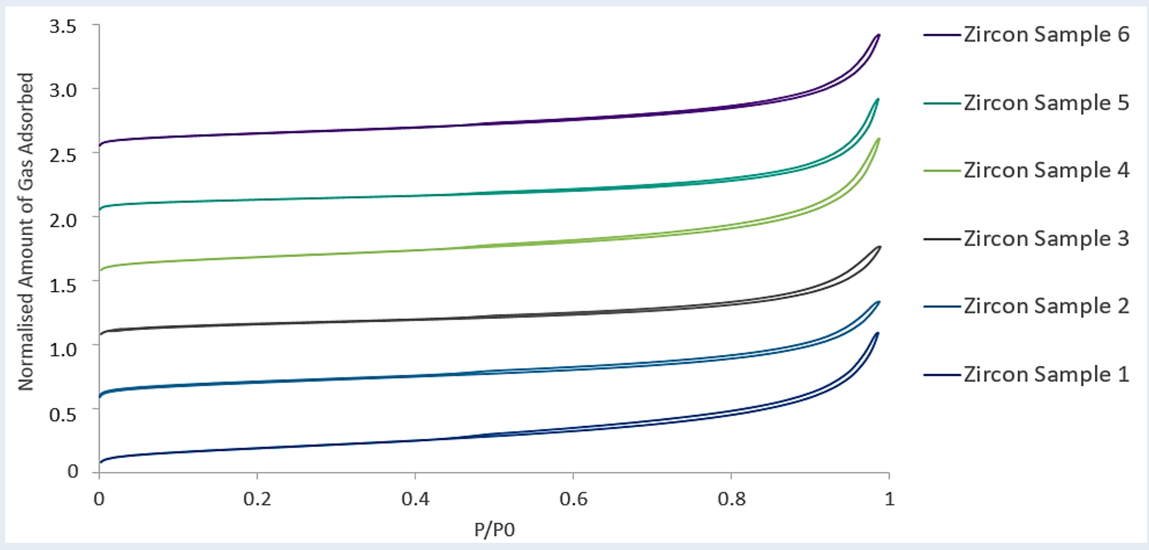

Figure 5: Adsorption –desorption isotherms for six differently sourced zircons.

5 Future Work

- Carry out powder characterisation experiments and develop slurry trials to undertake mechanical and dimensional testing for shell property analysis.
- Identify and rank the key raw material properties that have the greatest effect on turbine blade attributes.
- Propose a strategic method for dealing with unplanned changes in ceramic raw material properties that ensures equivalent turbine blade attributes.

6 References

[1] S. Jones, S. Bentley and P. Marquis, "Effect of refractory phase separation on investment mould integrity," British Ceramic Transactions, vol. 101, no. 3, pp. 100-105, 2002.
[2] Zircon Industry Association, "Technical handbook on zirconium and zirconium compounds", 2015.

UNIVERSITY OF BIRMINGHAM
Rolls-Royce
CENTRE FOR DOCTORAL TRAINING IN FORMULATION ENGINEERING
EPSRC Pioneering research and skills

UNDERSTANDING THE FINE GRINDING OF CALCIUM CARBONATE IN STIRRED MEDIA MILLS

Sophie Rimmer[A], Dr Andy Ingram[A], Dr Federico Alberini[A], Dr Richard Tamblyn[B]
A: Chemical Engineering, University of Birmingham, Edgbaston, Birmingham, B15 2TT
B: Imerys, Par Moor Centre, Par Moor Road, Par, PL24 2SQ

1. INTRODUCTION AND LITERATURE

Calcium carbonate has many uses; it is the most widely used mineral in the paint and paper industries, where it is used as a filler or extender (Mathur et al, 2016). However, small particles of calcium carbonate are required and fine grinding has a very low energy efficiency due to heat, vibration and noise losses. It is thought that only around 3-5% of the input energy is actually used for grinding (Moore, 2012). Hence, a lot of research is conducted in this area.

A lot of recent research uses PEPT (positron emission particle tracking) to look at flow patterns and how they change with operating parameters, such as:

- Grinding media size (see figure 2 example)
- Grinding media loading
- Impeller speed
- Vessel configuration, e.g. fitting of baffles

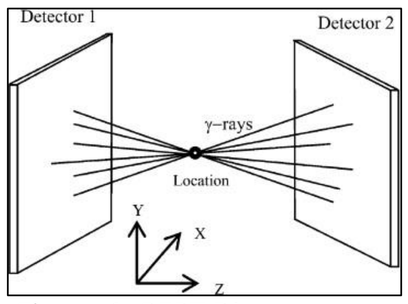

Figure 1: PEPT Diagram (Parker, Fan, 2008)

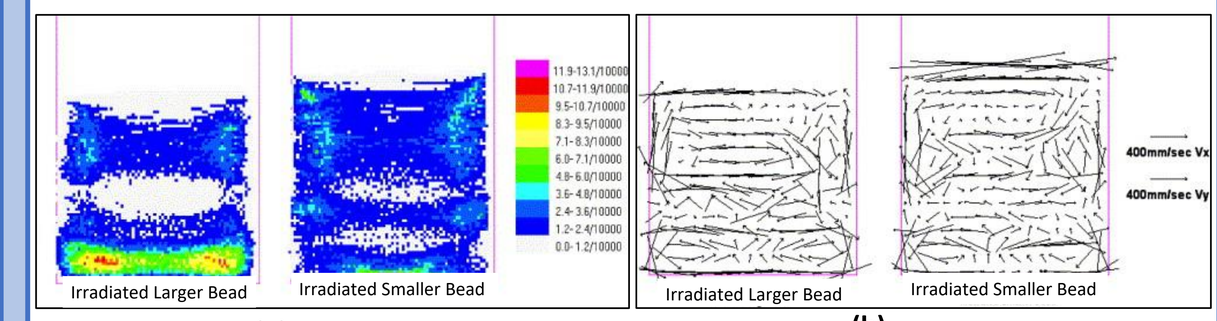

(a) **(b)**

Figure 2: PEPT Data Obtained by Barley et al (2004) - (a) Occupancy Plot, and (b), Velocity Streamline Plots

Another flow visualisation technique is PIV (particle image velocimetry), which enables the simultaneous tracking of many particles so has short experiment times. However, it is rarely used in stirred media mills because it requires a fully transparent set-up.

2. PROJECT AIMS

To further understand the flow inside stirred media mills.

- Develop transparent mimic fluid with the same viscosity as the calcium carbonate slurry.
- Use PIV to look at how the viscosity of the slurry affects flow patterns within the vessel.
- Compare PIV data with PEPT data.

To understand the issues involved in scale-up.

- Conduct tests at the pilot plant in Lixhe.
- Compare batch and continuous set-ups.

3. METHODS

Grinding
- Grind calcium carbonate until a pre-defined amount of energy has been consumed.
- Measure power draw throughout grind.

Measuring
- Find PSD using Mastersizer 2000.
- Find rheology using a vane rheometer.

Analysis
- Compare PSDs and power curves for different grinding conditions.
- Find suitable mimic fluid to use for PIV experiments.

4. EQUIPMENT

Figure 3: Lab Stirred Media Mill

Figure 4: Vane Rheometer

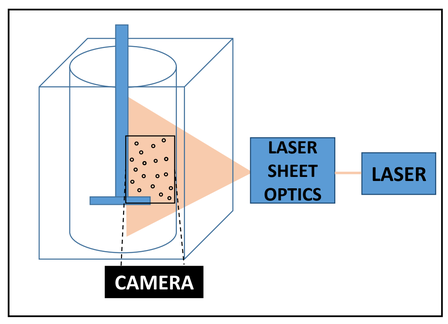

Figure 5: Basic PIV Set-Up

5. INITIAL RESULTS

Analysing the power curve during milling and relating it to changes in viscosity and particle size.

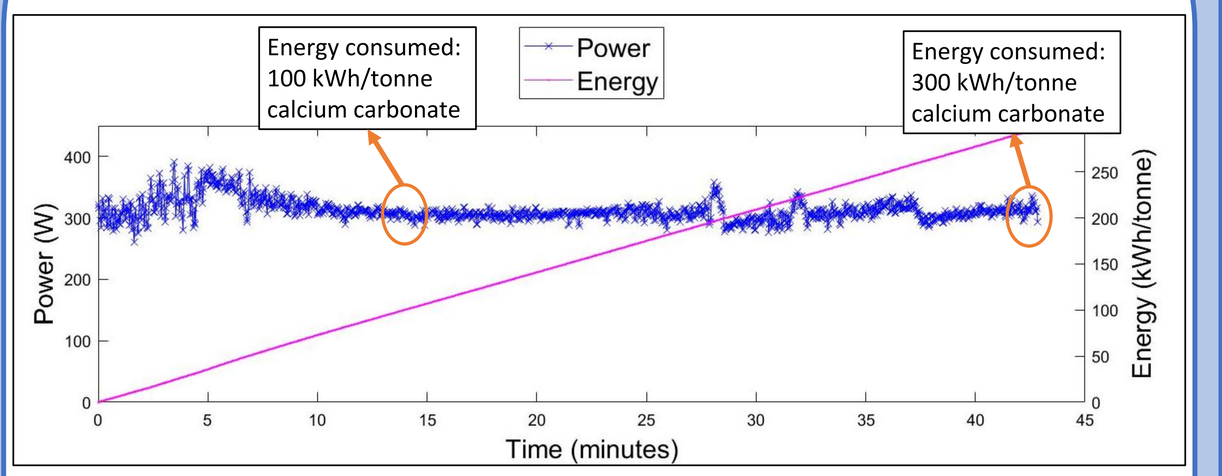

Figure 6: Power Curve with PSDs and Viscosity Data

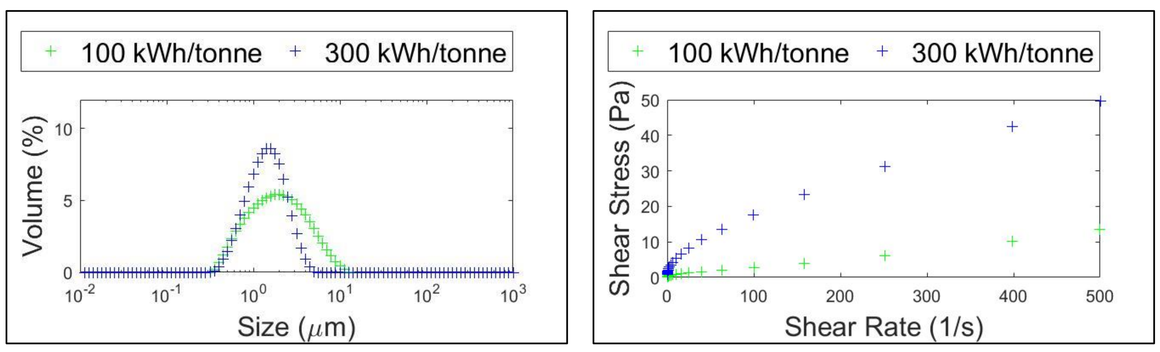

(a) **(b)**

Figure 7: (a) Particle Size, and (b) Viscosity Data at Corresponding Points on the Power Curve

- Initial power increase followed by a decrease due to temperature increase.
- Water added periodically to counteract power increases caused by the evaporation of water.

6. FURTHER RESEARCH

Compare the lab scale batch mill grinding with the continuous pilot plant grinding, including finding residence time distributions for continuous mills.

Compare data obtained using PIV to that obtained using PEPT.

Determine the rheology of calcium carbonate slurries at different points during grinding to find a suitable transparent mimic fluid for use with PIV.

7. REFERENCES

Barley, R. W; Conway-Baker, J; Pascoe, R.D; Kostuch, J, McLoughlin, B; D. J. Parker (2004) 'Measurement of the Motion of Grinding Media in a Vertically Stirred Mill Using Positron Emission Particle Tracking (PEPT) Part II' **Minerals Engineering,** Volume 15 (11-12), pp 1179-1187.

Mathur, N.K; Jakhar, S.R; Mathur, R (2016) 'Calcium Carbonate and Derived Products', International Journal of Science and Research, Volume 5(4), pp 2218-2133

Moore (2012) 'Dust to Dust', **International Mining,** [Online] Available at: http://www.min-eng.com/pdf/commin249.pdf [Accessed 1st February 2018]

Parker, D.J; Fan, X (2008) 'Positron Emission Particle Tracking – Application and Labelling Techniques, **Particuology,** Volume 6 (1), pp 16-23

Granule Characteristics After Twin Screw Granulation

Rachael Shinebaum [1], Hannah Batchelor [1], Ian Gabbott [2], Gavin K. Reynolds [2], Elaine H. Stone [3], Andrew Ingram [1]

[1] University of Birmingham, School of Chemical Engineering, Birmingham, UK
[2] Pharmaceutical Technology & Development, Astra Zeneca, Macclesfield, UK
[3] Merlin Powder Characterisation Ltd., Unit 8, The Wallows Industrial Estate, Fens Pool Avenue, Brierley Hill, West Midlands, DY5 1QA

Size Distribution

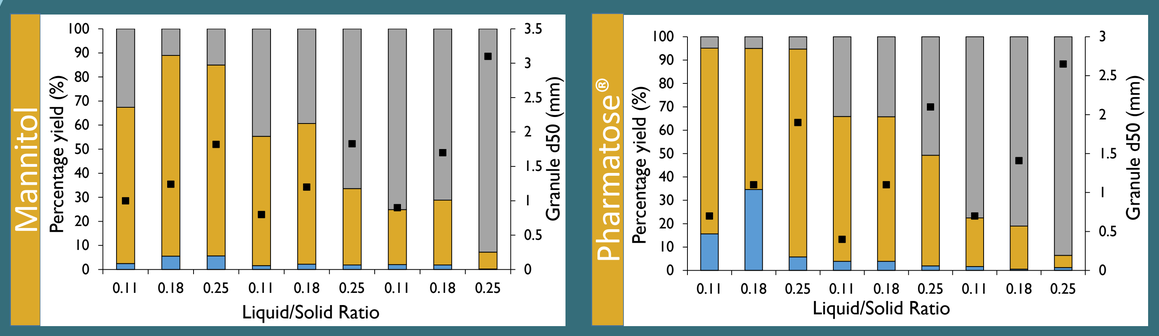

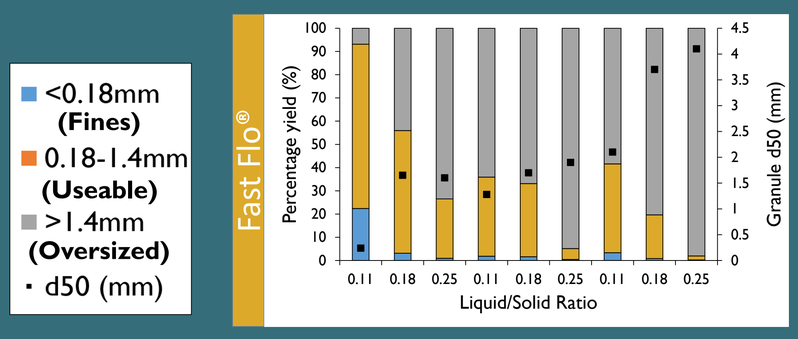

- <0.18mm **(Fines)**
- 0.18-1.4mm **(Useable)**
- >1.4mm **(Oversized)**
- d50 (mm)

Weight percentage data obtained from sieve analysis was used to show the yield of fine, usable and oversized granules for each batch. The figures above show the yield results for each material and median granule size (d50) based on granules from an entire batch. When liquid to solid ratio is increased, the quantity of oversized granules also increases, and the quantity of fines reduces to a negligible value.

Compression Behaviour

A hydraulic compression simulator was used to give high speed compaction data to provide information on granule tabletability. Tablets with a tensile strength of 2 MPa and greater [1] should be the target to ensure a robust product.

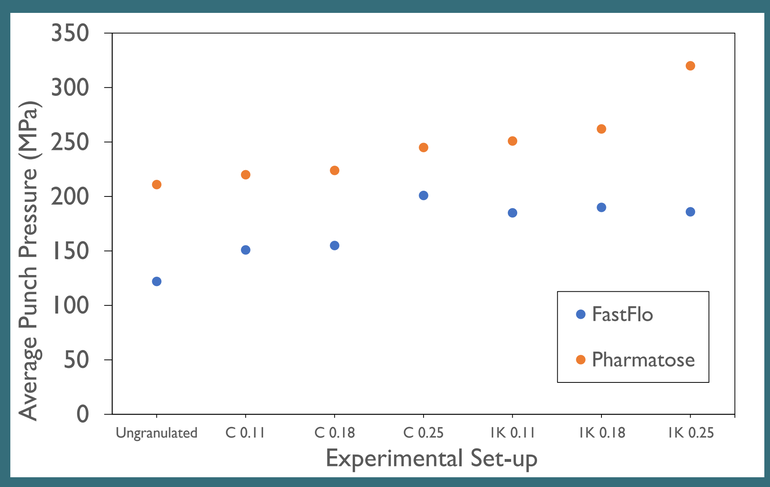

The graph above shows the average punch pressure required to produce a tablet with a tensile strength of 2 Mpa granule batches of Fast Flo® and Pharmatose®. Greater punch pressures are required as liquid content or kneading increases. Fast Flo® requires lower punch pressures than Pharmatose®.

Introduction

This study presents the key properties of granules produced via **Twin Screw Granulation (TSG)**, a continuous process which is gaining interest as an alternative to batch production techniques within the pharmaceutical industry. Three excipient materials with various properties were used to generate a fundamental understanding of the impact of process on granule properties.

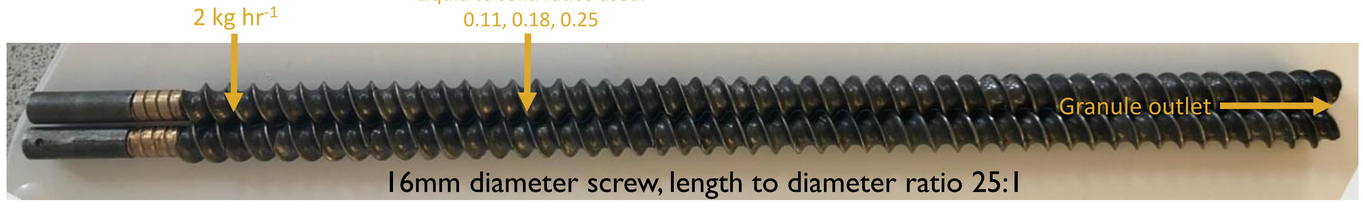

16mm diameter screw, length to diameter ratio 25:1

Three screw configurations were used:

- Conveying elements only
- 1 Kneading zone
- 2 Kneading zones

60° Forward kneading zone

Materials

Pharmatose® Lactose

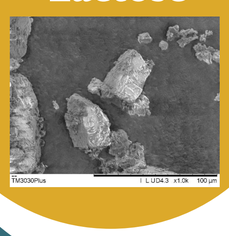

Distilled water

FastFlo® Lactose

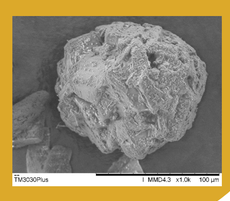

Pearlitol 160C® Mannitol

Granule Strength

Granule strength was measured by compressing granules via uniaxial bulk compression. The granule fracture strength was calculated using the Adam's equation shown below [2].

$$\ln P = ln\left(\frac{\tau}{\alpha}\right) + \alpha\varepsilon + ln[1 - exp(-\alpha\varepsilon)]$$

where P is the applied pressure (Pa), τ is the granule fracture strength (Pa), α is a material constant, ε is the natural strain. A plot of ε against ln P can be used to obtain values of α and τ from the intercept and gradient of the straight line fitted to the linear portion of the curve.

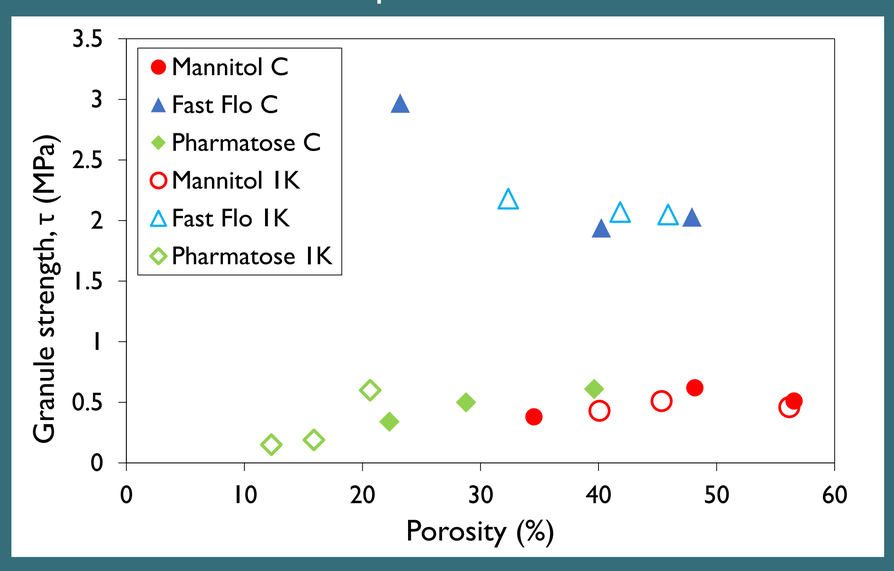

The graph above compares granule strength and porosity for batches of granules. The granule fracture strength of Fast Flo is higher than the other materials for a given porosity.

Porosity

Micro X-Ray Computer Tomography (micro-XRCT) was used to visualise the internal structure of granules and gain a percentage value for total porosity, this is shown in the matrix below. Granules were chosen at random from the 0.18mm-1.4mm size portion. As the number of kneading zones and liquid content increase, the granule porosity decreases.

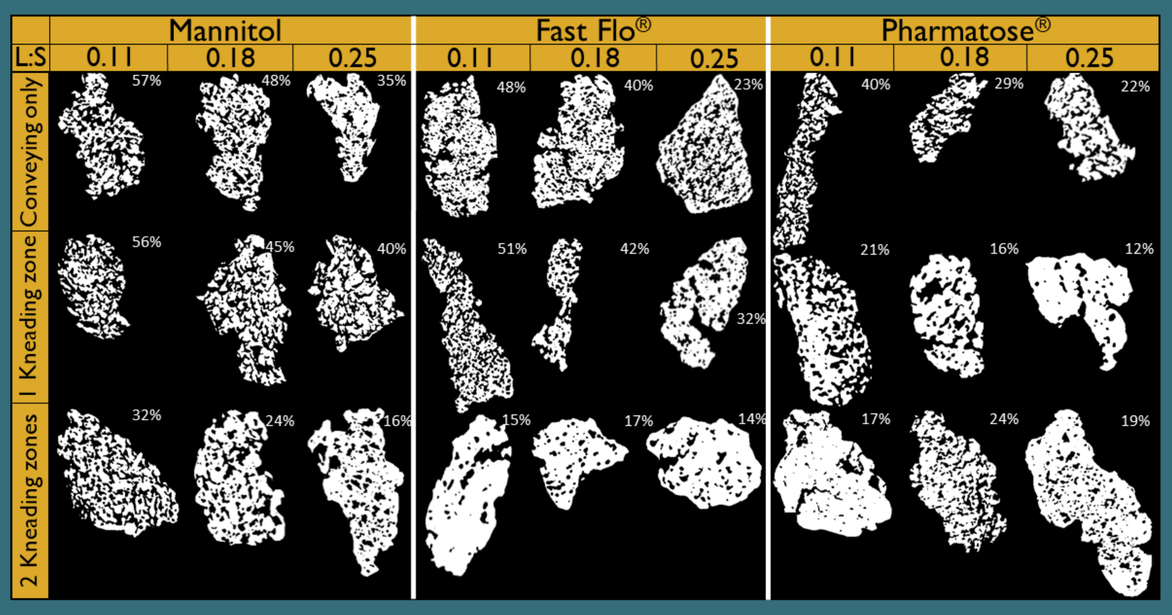

References

[1] Pitt, K. G. et al., 2015. Compression prediction accuracy from samll scale compaction studies to production presses. *Powder Technology*, Volume 270, pp. 490-493.
[2] Adams, M. J., Mullier, M. A. & Seville, J. P. K., 1994. Agglomerate strength measurement using a uniaxial confined compression test. *Powder Technology*, Volume 78, pp. 5-13.

Characterising dynamic powder flowability by the ball indentation method

M. Tirapelle, C. Hare

Department of Chemical and Process Engineering, University of Surrey, Guildford, GU2 7XH, UK
Department of Industrial Engineering, University of Padova, Via Marzolo 9, Padova, Italy

1. Introduction

Unreliable powder flow is a major problem during processing of powders, and as such there are a number of methods available for powder flow characterisation in quasi static condition.

Here we investigate the dynamic flow regimes by directly measuring the hardness with the Ball Indentation Method (BIM) and the flow energy using the FT4 Rheometer, both under a range of strain rates.

2. Materials and methods

The dynamic BIM simply consists of dropping a ball onto a cylindrical bed of previously consolidated powder. The impact of the ball is recorded with a high speed camera in order to determine the velocity, v_i, and the penetration depth, h, which is used to determine the unrelaxed volume (Eq. 2) and hence, the powder hardness H_d (Eq. 3).

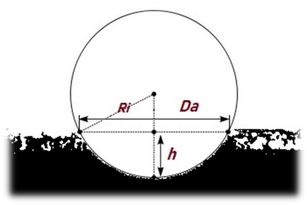

Figure 1. Bed surface profile.

$$h = R_i - \sqrt{R_i^2 - \left(\frac{D_a}{2}\right)^2} \qquad \text{(Eq. 1)}$$

$$U = \frac{\pi h}{6}\left[3\left(\frac{D_a}{2}\right)^2 + h^2\right] \qquad \text{(Eq. 2)}$$

$$H_d = \frac{M v_i^2}{2\,U} \qquad \text{(Eq. 3)}$$

The FT4 powder rheometer is used to apply the ball indentation method in quasi-static conditions, to allow comparison with the dynamic indentation method. The flow energy is measured in the FT4 using a range of tip speeds.

Fig. 2. FT4 powder rheometer [www.freemantech.co.uk].

$$H = \frac{F_{max}}{A} \qquad \text{(Eq. 4)}$$

Fig. 3. FT4 punch indenter.

The classification of the flow regimes is based on dimensionless strain rate γ* (Eq 5), where γ is the strain rate ($\gamma = v_i/r_i$).

Table 1. Classification of the flow regime.

Flow regime	
Quasi static	$\gamma^* < 0.15$
Intermediate	$0.25 < \gamma^* < 3$
Dynamic	$\gamma^* > 3$

$$\gamma^* = \gamma\sqrt{\left(\frac{d_p}{g}\right)} \qquad \text{(Eq. 5)}$$

3. Powder characterisation

Ti-pure R104 (Chemours) and lactose monohydrate GranuLac 140 (Meggle) are the powders used here.

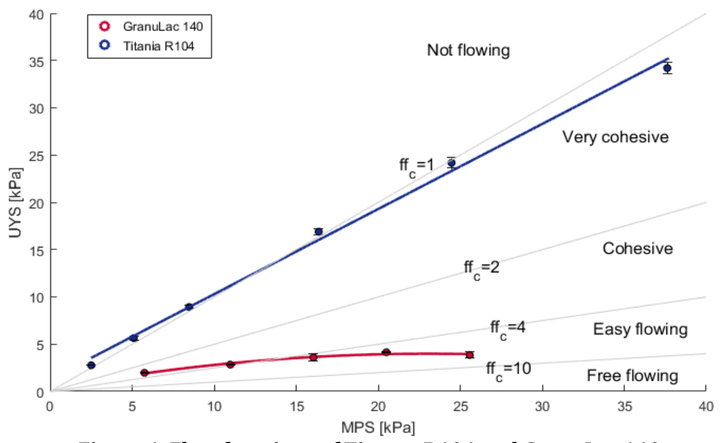

Figure 4. Flow functions of Ti-pure R104 and GranuLac 140.

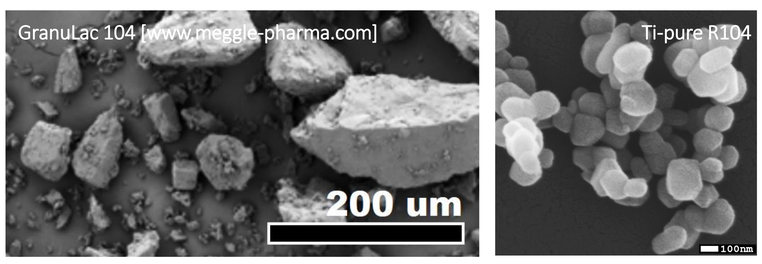

Figure 5. SEM micrographs.

Ti-pure R104 has a smaller particle size and a high tendency to agglomerate, and is very cohesive. GranuLac 140 instead is larger, has sharp-edges shape and can flow more easily.

Table 2. Particle diameter and Constraint factor.

	Ti-pure R104	GranuLac 140
dp [μm]	0.2-0.3	82.80
C factor	3.08	2.91

4. BIM results

The variation of the hardness with the strain rate is considered for different materials and size, and a range of drop heights.

With **Ti-pure R104**, because of the smaller particle dimension (d=0.2-0.3 μm), it was possible to evaluate the hardness only in the quasi-static regime and in the uncertain boundary before the intermediate regime. In that range of dimensionless strain rate, γ*, the hardness measurement are not effected by the indenter size (Figure 6) as long as the wall effect of the die is avoided.

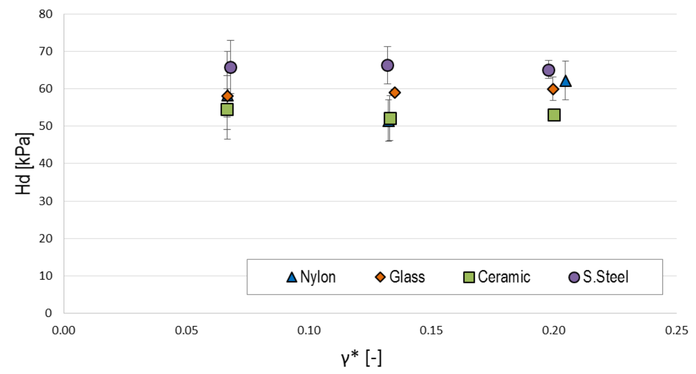

Figure 6. Hardness as a function of γ* using different indenters (v_i=1.983±0.015 m/s, powder compaction=20 kPa).

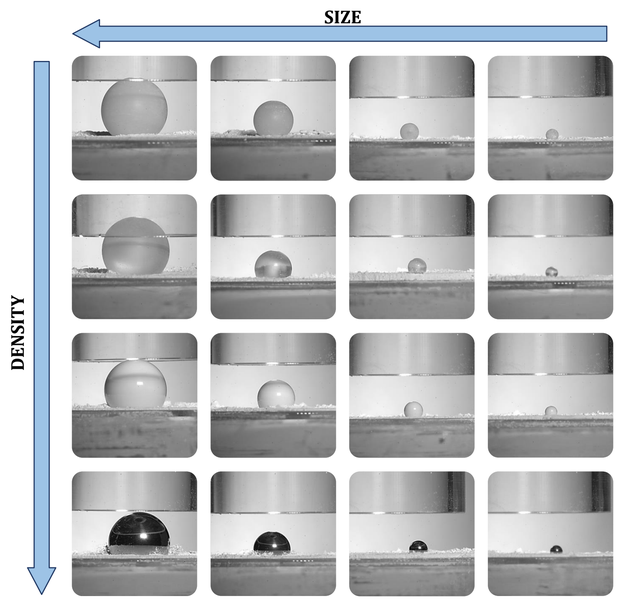

Figure 7. Bed surface profiles (v_i=1.983±0.015 m/s, powder compaction=20 kPa).

Indenters of different density give different results because, as shown by quasi-static indentation, hardness increases at greater dimensionless penetration depths (Figure 8).

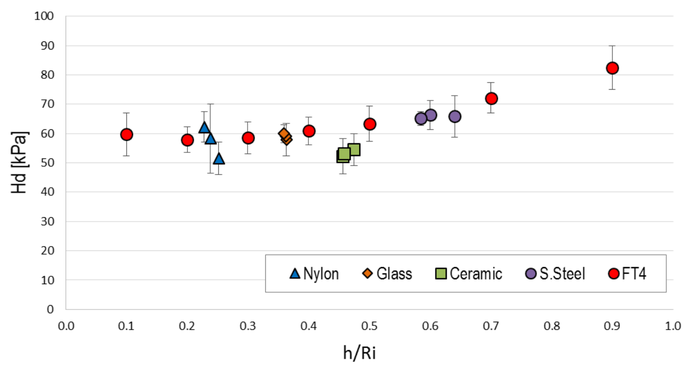

Figure 8. Variation of hardness with dimensionless penetration depth. Comparison with the FT4 measurements.

With **GranuLac 104**, because of the larger particle size (d50=82.8 μm), the hardness was evaluated in a wider range of γ*. The results show that the hardness increases with the strain rate when the powder behaves cohesively (Figure 9), whereas it is constant when it can flow easily (Figure 10).

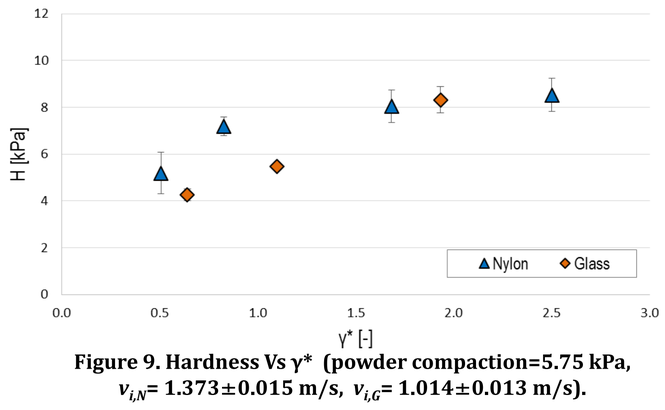

Figure 9. Hardness Vs γ* (powder compaction=5.75 kPa, $v_{i,N}$= 1.373±0.015 m/s, $v_{i,G}$= 1.014±0.013 m/s).

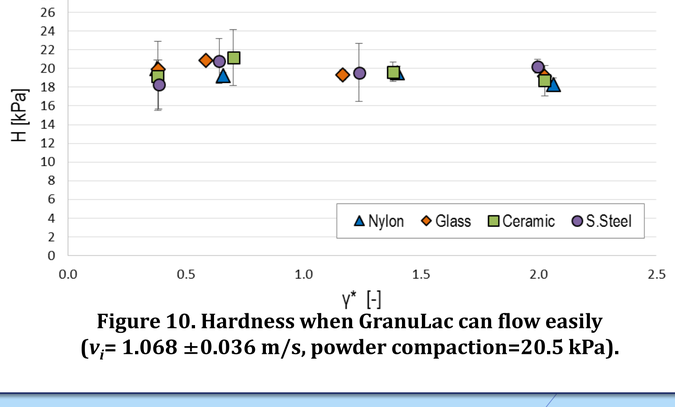

Figure 10. Hardness when GranuLac can flow easily (v_i= 1.068 ±0.036 m/s, powder compaction=20.5 kPa).

5. Flow energy measurements

The work done by the FT4 blade to penetrate the powder bed whilst rotating anticlockwise with a 50° helix angle is evaluated at different tip speeds. To have comparable results, the flow energy (Eq. 6) has been calculated always considering the same penetration depth of 20 mm.

$$E = \int_0^h \left(\frac{T}{R\tan(\alpha)} + F\right) dh \qquad \text{(Eq. 6)}$$

For **Ti-pure R104** this method has been performed both on a not consolidated powder and on a bed compacted to 5 kPa. In the latter case the flow energy increases with increasing tip speed, whilst in the former case the flow energy decreases slightly with increasing tip speed.

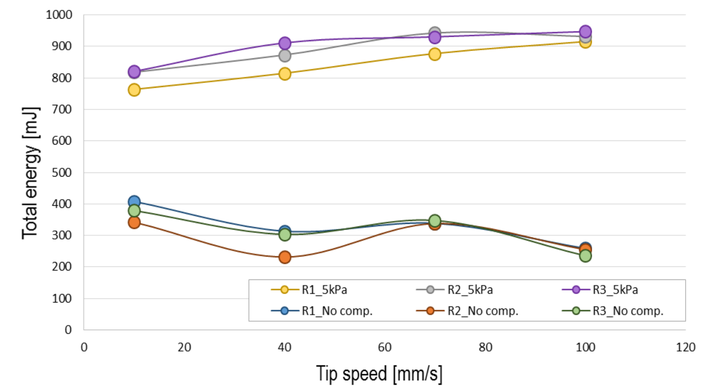

Figure 11. Energy consumed at different tip speed. Ti-pure has been compacted at 0 and 5 kPa.

For **GranuLac 104** the flow energy on a bed compressed to 5.75 kPa has been evaluated. Considering the entire range of tip speeds investigated, the powder shows a Newtonian or pseudo-plastic behaviour.

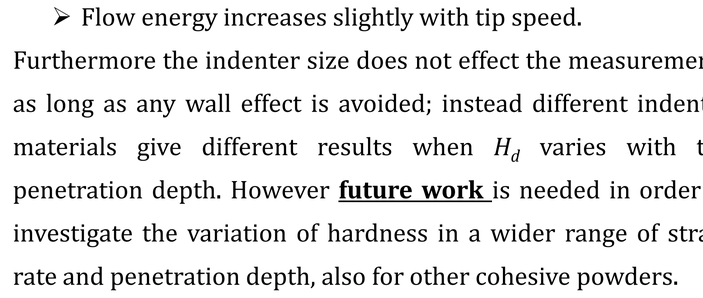

Figure 12. Energy consumed at different tip speed considering a 5.75 kPa compacted bed of GranuLac.

6. Conclusion and future work

Results obtained with the BIM show that **for cohesive powders**:

- H_d does not vary in quasi-static conditions;
- H_d increases in the intermediate regime;
- Dependency of flow energy on tip speed varies between compacted and uncompacted states.

For **free flowing materials**:

- H_d remains constant in the quasi-static and intermediate regimes;
- Flow energy increases slightly with tip speed.

Furthermore the indenter size does not effect the measurements as long as any wall effect is avoided; instead different indenter materials give different results when H_d varies with the penetration depth. However **future work** is needed in order to investigate the variation of hardness in a wider range of strain rate and penetration depth, also for other cohesive powders.

7. References

[1] G. I. Tardos, S. McNamara, I. Talu, Slow and intermediate flow of a frictional bulk powder in the Couette geometry, Powder Technology, 131 (2003) 23–39.

[2] A. Hassanpour, M. Ghadiri, Characterisation of Flowability of Loosely Compacted Cohesive Powders by Indentation, Particle & Particle Systems Characterisation, 24 (2007) 117–123.

[3] Y. Tirupataiah, G. Sundararajan, The volume of the crater formed by impact of a ball against flat target materials-the effect of ball hardness and density, Int. J. Impact Eng, 9 (1990) 237-246.

[4] Freeman tech. website: www.freemantech.co.uk

The ERASMUS+ program of the European Union is gratefully acknowledged.

Contact:
mt00895@surrey.ac.uk (M. Tirapelle),
c.hare@surrey.ac.uk (C. Hare)

Development of a New Apparatus for the Investigation of Particles Momentum Transfer in Fluidised Beds

Tobias Matthaeus Piepke[1-2], Stefan Pollak[2], Lyes Ait Ali Yahia[1], Raffaella Ocone[1]
[1]Heriot-Watt University Edinburgh Campus (Edinburgh, Scotland, EH14 4AS)
[2]Ruhr-Universität Bochum (Universitätsstr. 150, 44801 Bochum, Germany)

Introduction: Fluidised bed technology is largely employed in the process industries. Despite their various applications, such as reactors, combustors or dryers [1], there is still no accurate method to calculate the momentum transfer in fluidised beds [2]. Against this background, the central question, that motivates this research project, is whether it is possible to characterise the particles momentum transfer in fluidised beds using the same measurement principle as the one used in a Coaxial-Cylinder-Viscometer for liquids.

Fluidised Bed

- Particles are fluidised by gas or liquid
- Fluidisation starts when the force from the airflow ($\Delta P \cdot A$) is able to raise the mass of particles in the bed:
$$\Delta P \cdot A = m \cdot g$$
- The type of fluidisation mainly depends on particle diameter and density according to Geldart´s Powder Classification

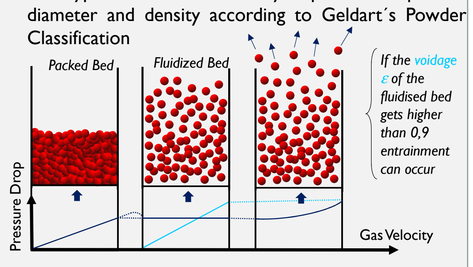

Shear Stress

- The shear stress, τ, is defined as the force F that is needed to shear a fluid (planar Couette-flow) or particles in a defined cross sectional area A:
$$\tau = F/A$$
- For particles in a packed bed the shear stress and the angle of internal friction can be determined with a shear test
- For particles in a fluidised bed there is no accepted method available to characterise the shear stress

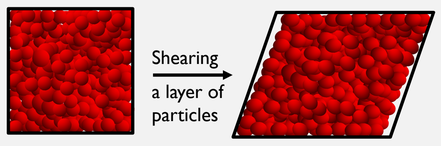

Momentum Transfer

- In fluids and gases the momentum is being transferred on a molecular scale
- In a fluidised bed the momentum is transferred between particles and between particles and fluid
- Plastic and elastic contributions can be present

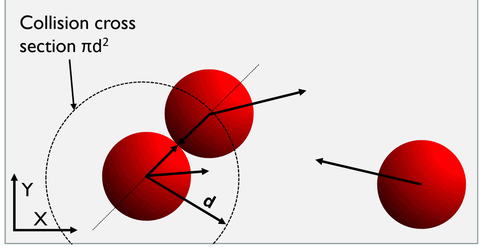

Taylor-Couette Flow

- The "fluid" is placed in the gap between two cylinders rotating relatively to each other
- The torque, T, due to friction can be measured
- The shear stress represents the friction between two layers
- Distinction between non-linear and linear velocity profiles (narrow gap – $\delta_{CC}=R_2/R_1 < 1{,}0847$) can be detected

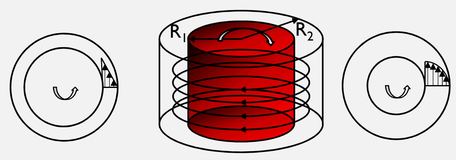

(Apparent) Viscosity

- The viscosity describes the resistance against a deformation of the fluid due to the shear stress
- The viscosity can be time (in-)dependent and is a function of the shear rate which depends on the rotational velocity of the cylinder
- Apparent viscosity in a fluidised bed depends on the load and shape of the solid particles

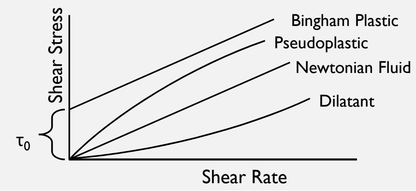

1. **Silica** (40µm-63µm – Geldart Group A)
2. **Glass Beads** (200µm – Geldart Group B – further research)
3. **Glass Beads** (500µm – Geldart Group B – further research)

Characterisation of the Fluidised Bed

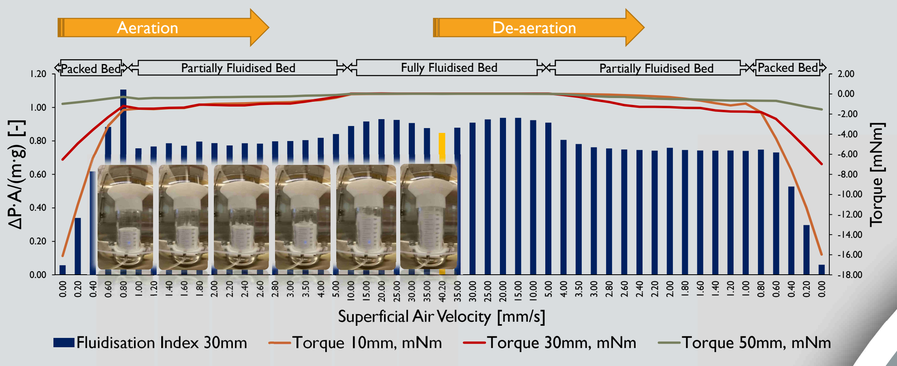

- Measurement with the FT4 48mm impeller (tip-speed 100mm/s)
- Evaluation of torque for packed and partially fluidised bed (Silica)
- Evaluation of the minimum fluidisation velocity U_{mf}
- $U_{mf,Silica,63\mu m}$ = 8,3mm/s (Ergun-Equation[1], ε_{mf}=0.5)
- $U_{mf,Silica,63\mu m}$ = 3.0mm/s (Wen and Yu Equation[1], ε_{mf}=0.5)
- Torque becomes almost 0mNm for the fully fluidised bed

➢ **Virtual Couette Cell for the FT4**

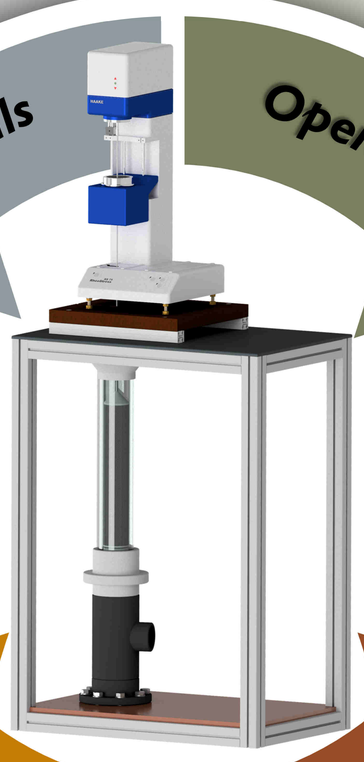

Fundamentals

Operating Principle

Apparatus Design

Comparison

Virtual Couette-Cell

- Height 70mm
- Diameter 36mm
- Gap inner-outer cylinder 7mm

Why a Virtual Couette-Cell?

- Cylindrical geometry is well known (for liquids)
- Defined shear-zone
- Cylindrical geometry is comparable to the FBR

Evaluation of the apparent torque and the shear stress

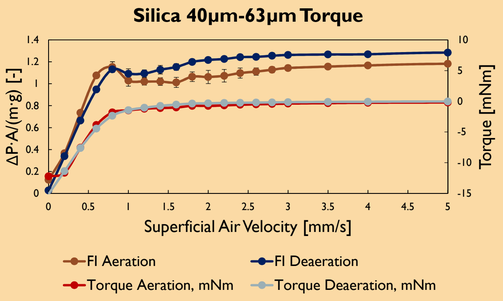

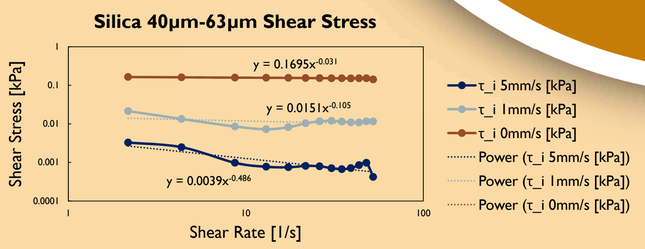

$$Shear\ Stress^{[3]} \tau_i = \frac{M}{2\pi \cdot R_i^2 \cdot h} \text{ and } Shear\ Rate^{[3]} \dot{\gamma}_i = \frac{2 \cdot R_a^2}{R_a^2 - R_i^2} \cdot \omega$$

Comparison of the apparent torque

- The measured torque will be compared with the results of the FBR in order to validate it
- The trend of the curve will be compared to known liquid-solid and gas-solid flow behaviour
- Comparison for the packed bed and beginning fluidisation for different shear rates

The inner cylinder rotates in the fluidised bed
- A layer of particles is glued at the inner cylinder (Particles Momentum Transfer)
- Inner cylinder with a known roughness (Particle-Wall Interactions)

The torque is measured with the Haake Rheostress RS75
- Particle-particle or particle-wall momentum transfer
- Molecular momentum transfer through the airflow

The torque is converted into the shear stress

The shear stress and the shear rate are converted into an apparent viscosity of the fluidised bed

→ Characterisation of the fluidised bed through the apparent viscosity

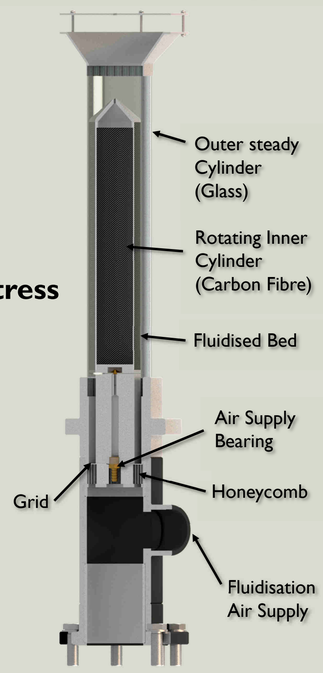

Haake Rheostress RS75

- Torque measurement between **5·10⁻³ mNm** and **100 mNm**
- Rotational velocities between **0.1 rpm** and **580 rpm**

Geometrical determination of the Apparatus

- Diameter Inner Cylinder = 80mm
- Height Inner Cylinder = 450mm
- Gap Inner-/Outer Cylinder =14.5mm

$T_{min} = 5 \cdot 10^{-3}\ mNm$ ← $\tau_{min} = 0.006$Pa ← $\tau = \frac{T}{2 \cdot \pi \cdot R_i^2 \cdot H}$ → $\tau_{max} = 22.105$Pa → $T_{max} = 100\ mNm$

	Min. shear rate (0.045 1/s)	Max. shear rate (263.318 1/s)
Smallest Viscosity	$\eta(min) = \frac{\tau(min)}{\dot{\gamma}(min)} = 0.137$ Pa s	$\eta(min) = \frac{\tau(min)}{\dot{\gamma}(max)} = 2.361 \cdot 10^{-5}$ Pa s
Largest Viscosity	$\eta(\max) = \frac{\tau(max)}{\dot{\gamma}(min)} = 486.896$ Pa s	$\eta(\max) = \frac{\tau(max)}{\dot{\gamma}(max)} = 0.084$ Pa s

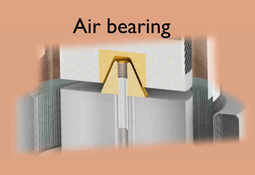

Bearing:
- The needle bearing can be substituted with an air bearing to avoid friction

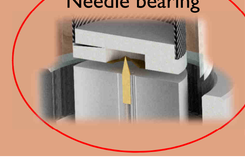

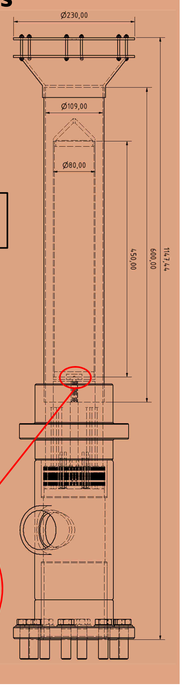

Conclusions

- **Comparison** and **Validation** of the FBR for the packed bed and beginning fluidisation for Silica (40µm-63µm)
  - Use the same particles (40µm-63µm Silica) in order to minimise influence of the particles sphericity
  - The cohesion can be shown for the pressure drop – superficial air velocity diagram
  - Influence of the rotating geometry on the fluidised bed
- **Measurements with spherical particles** (200µm and 500µm glass beads) necessary to validate the FBR for larger particle diameter and for the fully fluidised bed
- **The Virtual-Couette-Cell** allows the evaluation of the **shear stress** in the fluidised bed
  - Shear stress for packed bed can be written as a function of the apparent viscosity η and the shear rate $\dot{\gamma}$:
$$\tau = \tau_0 + \dot{\gamma} \cdot \eta(\dot{\gamma}) \text{ with } \eta(\dot{\gamma}) = c\dot{\gamma}^{-1}$$
- **Developed a FBR that theoretically can measure a wide range of gas-solid mixtures**

Further Research

- **Practical Measurements** with the FBR at Ruhr-Universität Bochum
  - Measurements with spherical glass beads (200µm and 500µm)
  - Evaluating particle-particle and particle-wall momentum transfer
  - Evaluating cohesion and the effects of the rotating inner cylinder
- **Measurement of the apparent torque** for the FBR and conversion to **shear stress**
- **Shear stress** will be converted to **the apparent viscosity** (Non-Newtonian)
  - Sperate determination of $\boldsymbol{\tau_0}$ **and** $\boldsymbol{\dot{\gamma} \cdot \eta(\dot{\gamma})}$ for the FBR and comparison to the Virtual-Couette-Cell (FT4)
- **Practical measurements and validation of the results of the FBR**

[1] M. S. Ray, "Chemical Engineering, Volume 2: Particle Technology and Separation Processes, 4th edn, by J.M. Coulson and J.F. Richardson. Pergamon Press, Oxford, UK. 1991. 968 pp. ISBN 0-08-037957-5," *Dev. Chem. Eng. Miner. Process.*, vol. 1, no. 2–3.
[2] R. Borghi and F. Anselmet, *Turbulent Multiphase Flows with Heat and Mass Transfer*. John Wiley & Sons, 2013.
[3] D. S. Viswanath, T. Ghosh, D. H. L. Prasad, N. V. K. Dutt, and K. Y. Rani, *Viscosity of Liquids: Theory, Estimation, Experiment, and Data*. Springer Netherlands, 2007.
[4] P. Coussot, *Rheophysics: Matter in all its States*. Springer International Publishing, 2014.
[5] R. B. Bird, W. E. Stewart, and E. N. Lightfoot, *Transport Phenomena*. John Wiley & Sons, 2007.

Gravity and Suction Filling of Pharmaceutical Powders

International Fine Particle Research Institute

Anastasiya Zakhvatayeva, Colin Hare and Chuan-Yu (Charley) Wu

Department of Chemical and Process Engineering, University of Surrey, Guildford, GU2 7XH, U.K.

C.Y.Wu@surrey.ac.uk

1. Introduction

Die filling is a critical process step in pharmaceutical tablet manufacturing. Mass and content uniformity of the tablets as well as the final production throughput depend upon the die filling performance of pharmaceutical formulations.

It is therefore important to understand how powder characteristics and die filling systems influence the efficiency of die filling.

2. Materials

The study was performed using seven excipients commonly used in the manufacturing of solid oral dosage forms.

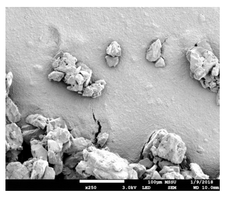

Lactose monohydrate

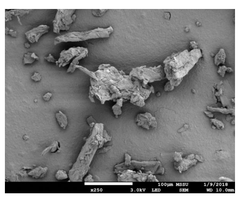

MCC DG

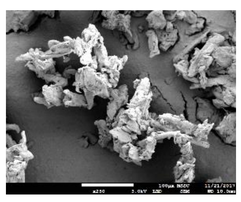

MCC PH101

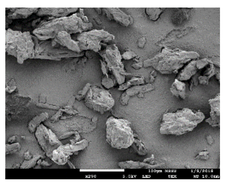

MCC PH102

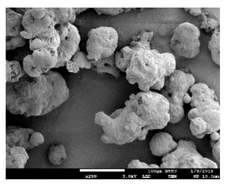

Mannitol

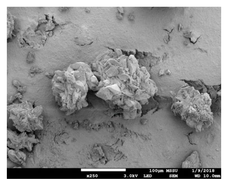

Dicalcium phosphate anhydrous

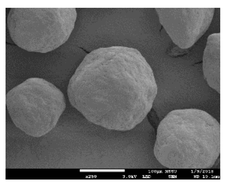

MCC CP102

3. Experimental set up

The die filling behaviour of the powders was explored using two types of die filling systems:

a)Linear die filling system (Fig.1), consisting of:

- moving feeder(*fill shoe*),

- stationary die.

b) Rotary die filling system (Fig.2), consisting of:

- stationary fill shoe,

- moving die (Fig.3).

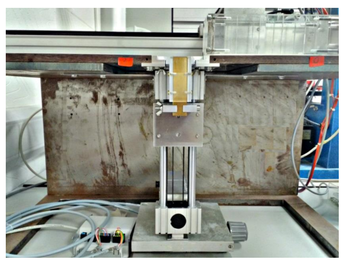

Fig.1

Fig.2

The linear die filling system is also equipped with a vertical displacement drive, connected to a piston (Fig.4). This configuration is used to investigate the suction filling mechanism.

Fig.3

Fig.4

3. Powder characterization

The following powder properties were investigated:

- Morphology (SEM)
- Mass flow rate (Flodex)
- Particle size distribution (Sympatec)
- Specific Energy (FT4)
- Air permeability (FT4)
- Cohesion and flow function (FT4).

The variation of the fill ratio with the fill speed was analysed for the two devices. The suction filling was further investigated for Lactose, MCC PH102 and MCC CP102 on the linear device.

4. Results

Linear die filling vs rotary die filling

Linear die filling

The top sequence is typical of cohesive powders (intermittent flow) like Lactose monohydrate, MCC DG and MCC PH101.

The sequence in the middle describes a more freely flowing MCC PH102.

The bottom sequence is typical of less cohesive, free flowing DCPA, Mannitol and MCC CP102.

Rotary die filling

The flow profiles are similar to those observed on the linear system, but the efficiency of die filling is on average higher (see graphs below).

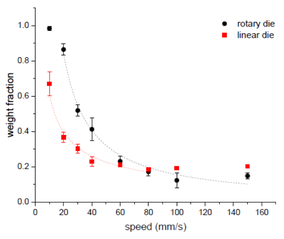

Lactose monohydrate

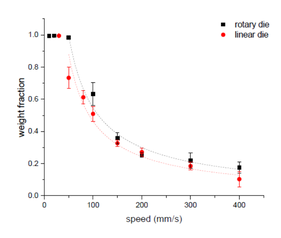

MCC PH102

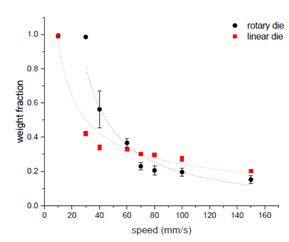

MCC DG

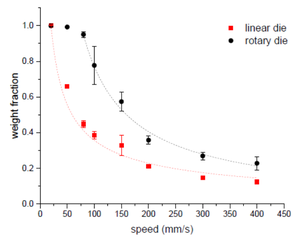

Mannitol

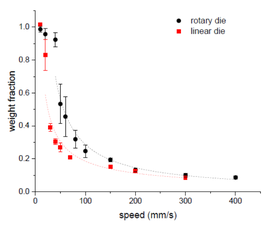

MCC PH101

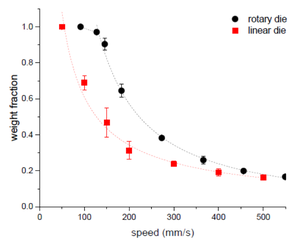

DCPA

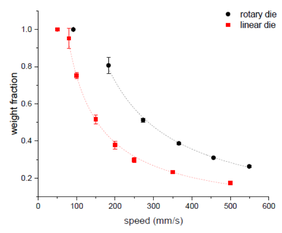

MCC CP102

The rotary die filling system performs better than the linear one:

- At low values of fill speed, the fill ratio tends to be high for both the systems.
- As the speed increases the difference between the linear and the rotary devices in terms of fill ratio becomes more evident for free flowing powders (See mannitol, DCPA and MCC CP102).

Gravity die filling vs suction filling

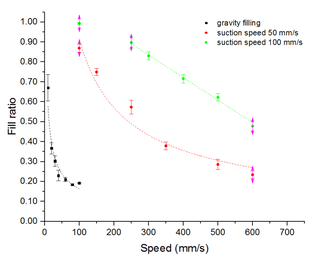

Lactose monohydrate

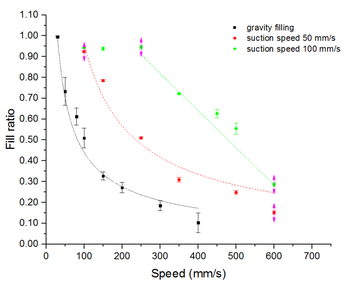

MCC PH102

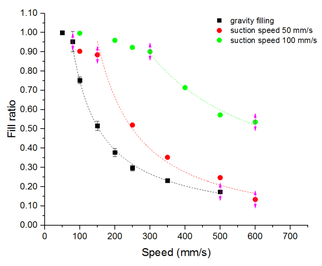

MCC CP102

The efficiency of die filling increases significantly with suction filling. This increase is particularly evident for more cohesive Lactose and MCC PH102, although the filling efficiency of such free flowing and coarse product as CP102 are also improved by the suction.

Influence of powder properties on die filling efficiency

The correlation of the critical filling velocities [1] of different powders with such powder properties as average particle size (d_{50}), specific energy, pressure drop, cohesion and flow function were explored.

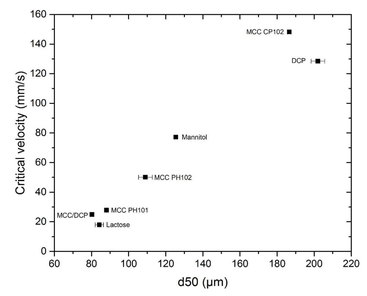

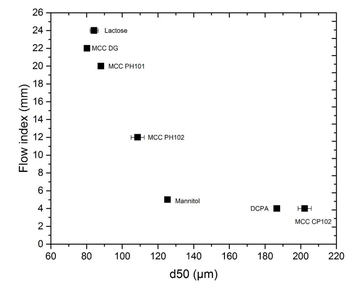

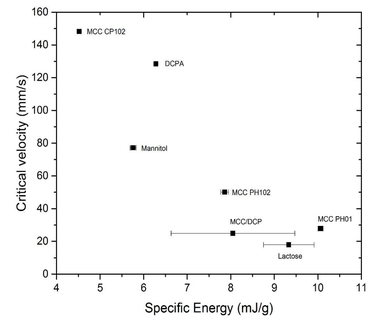

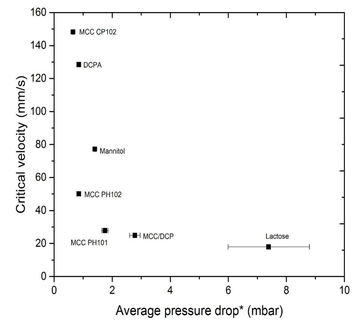

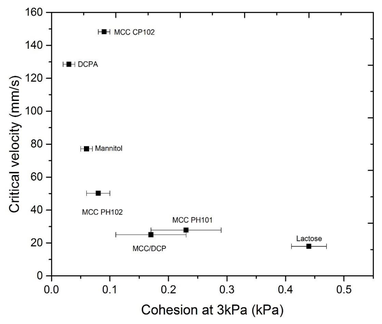

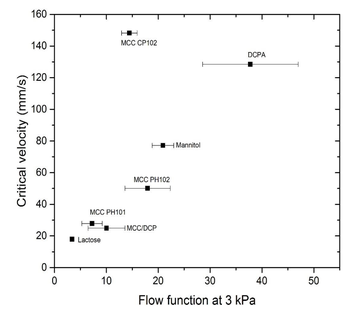

5. Conclusions

1. For gravity filling, the rotary system performs better than the linear system. But at higher speeds, the effect of cohesion prevails.
2. The suction filling improves significantly the fill ratio: especially for cohesive powders with smaller particle size, as has been observed by Mills et al [2].
3. Higher critical fill velocity are associated with larger particle size and higher flow function value, lower specific energy, average pressure drop and cohesion.

6. Future work

- ❑ Evaluation of the impact of powders properties on the efficiency of suction die filling.
- ❑ Study of multicomponent blends, with the focus on uniformity of model API distribution within the die and the influence of process parameters (fill and suction speed) on the content uniformity.
- ❑ Investigation of forced die filling, for which a paddle powder feeder will be designed and fitted into the die filling apparatus. The die filling efficiency will then be explored.

7. Reference

[1] Wu, C. Y., Dihoru, L., & Cocks, A. C. F. (2003). The flow of powder into simple and stepped dies. *Powder Technology*, *134*(1–2), 24–39.

[2] Mills, L. A., & Sinka, I. C. (2013). Effect of particle size and density on the die fill of powders. *European Journal of Pharmaceutics and Biopharmaceutics*, *84*(3), 642–652.

[3] Freeman, R., & Fu, X. (2008). Characterisation of powder bulk, dynamic flow and shear properties in relation to die filling. Powder Metallurgy, 51(3), 196–201.